Journal of Cardiology 64 (2014) 488–495

Journal of Cardiology

journal homepage: www.elsevier.com/locate/jjcc

Original article

The role of integrated backscatter intravascular ultrasound in characterizing bare metal and drug-eluting stent restenotic neointima as compared to optical coherence tomography

Kastsumasa Sato (MD)[a,b,*], Charis Costopoulos (MD)[a], Hideo Takebayashi (MD, PhD)[b], Toru Naganuma (MD)[a], Tadashi Miyazaki (MD)[a], Kenji Goto (MD)[b], Hiroki Yamane (MD)[b], Arata Hagikura (MD)[b], Yuetsu Kikuta (MD)[b], Masahito Taniguchi (MD)[b], Shigeki Hiramatsu (MD, PhD)[b], Hiroshi Ito (MD, PhD, FJCC)[c], Antonio Colombo (MD)[a], Seiichi Haruta (MD)[b]

[a] *Interventional Cardiology Unit, EMO-GVM Centro Cuore Columbus, Milan, Italy*
[b] *Fukuyama Cardiovascular Hospital, Fukuyama, Japan*
[c] *Department of Cardiovascular Medicine, Okayama University Graduate School of Medicine, Dentistry and Pharmaceutical Sciences, Okayama, Japan*

ARTICLE INFO

Article history:
Received 24 December 2013
Received in revised form 5 March 2014
Accepted 7 March 2014
Available online 29 April 2014

Keywords:
Neointima
In-stent restenosis
Integrated backscatter intravascular ultrasound
Optical coherence tomography

ABSTRACT

Background: To evaluate the role of integrated backscatter intravascular ultrasound (IB-IVUS) in assessing the morphology of neointima in bare-metal stent (BMS) and drug-eluting stent (DES) restenosis as compared to the gold-standard, optical coherence tomography (OCT).
Methods: A total of 120 cross-sections were evaluated by IB-IVUS and OCT at five cross-sections from 24 patients (24 lesions): at the minimal lumen area (MLA) and at 1 and 2 mm proximal and distal to the MLA site in 24 lesions (9 treated with DES and 15 treated with BMS). IB-IVUS and OCT findings were analyzed according to the time at which restenosis was identified (early <12 months and late ≥12 months) and the stent type.
Results: IB-IVUS was found to correctly characterize the neointima of both BMS and DES in-stent restenosis (ISR) as compared to OCT. The overall agreement between the pattern of ISR neointima by IB-IVUS and that by OCT was excellent (kappa = 0.85, 95% CI 0.76–0.94). Late DES ISR was characterized by more non-homogeneous, low backscatter and lipid-laden neointima, as compared to the BMS equivalent (BMS vs. DES, 45.0% vs. 80.0%, $p < 0.01$; 51.7% vs. 85.0%, $p = 0.008$; 33.3% vs. 65.0%, $p < 0.01$, respectively).
Conclusions: IB-IVUS assessment of the ISR neointima pattern appears to provide similar information as the gold-standard OCT in patients with stable angina. Both modalities suggested that late DES restenosis is characterized by a non-homogeneous lipid-laden neointima.

Introduction

Optical coherence tomography (OCT) and integrated backscatter intravascular ultrasound (IB-IVUS) can provide excellent tissue characterization of coronary plaque morphology [1,2]. In vivo OCT images can provide more detailed structural information of coronary atherosclerotic plaques as compared to conventional intravascular ultrasound (IVUS). Previous studies have demonstrated that the OCT findings regarding atherosclerotic plaque composition correlate well with those obtained from histological samples [2]. Attempts to characterize the coronary atherosclerotic plaque composition have also been made with other modalities including IB-IVUS [3,4]. A prior OCT study by our group has demonstrated that the differences in the neointima exist at different restenotic phases and between different stent types [5,6]. However, quantitative evaluation of the neointima morphology at early and late restenosis and according to stent type [bare-metal stent (BMS) vs. drug-eluting stent (DES)] has not been well characterized by IB-IVUS. The purpose of this study was to examine the role of IB-IVUS in characterizing the neointima of in-stent restenotic (ISR) segments according to the time at which the restenosis was identified

* Corresponding author at: EMO-GVM Centro Cuore Columbus, 48 Via M. Buonarroti, 20145 Milan, Italy. Tel.: +39 02 4812920; fax: +39 02 48193433.
E-mail address: katsumasaz4@yahoo.co.jp (K. Sato).

http://dx.doi.org/10.1016/j.jjcc.2014.03.007
0914-5087/

(early <12 months or late phase ≥12 months) and the stent type and compare these findings to those obtained by the gold-standard OCT.

Methods

Study patients

The study population was recruited from a total of 194 patients with stable angina who were admitted to Fukuyama Cardiovascular Hospital from June 2009 to November 2011 for target lesion revascularization (TLR). Among them, 24 consecutive patients who subsequently underwent TLR using both IB-IVUS and OCT were enrolled in this study. All patients had ischemic symptoms or evidence of myocardial ischemia in the presence of ≥75% diameter stenosis at follow-up angiography. We excluded patients with acute coronary syndrome necessitating primary percutaneous intervention and stent edge restenosis. The study protocol was approved by the institutional ethics committee of Fukuyama Cardiovascular Hospital, and written consent was obtained from all patients prior to the procedure.

Gray-scale IVUS and IB-IVUS measurements

IB-IVUS and gray-scale IVUS examinations for ISR lesions were performed before any intervention and after the intracoronary administration of isosorbide dinitrate (1–2 mg). The transducer was advanced into the distal reference segment, and an imaging run was performed back through the stent to coronary ostium using a motorized transducer pullback (0.5 mm/s) system.

Gray-scale IVUS and ultrasound signals were acquired with a commercially available IVUS imaging system (VISIWAVE, Terumo, Tokyo, Japan) using a 43-MHz mechanically rotating IVUS catheter (View IT, Terumo). During the pullback, images were obtained at 30 frames/s. All IVUS imaging data were stored in the console. For offline analysis, digital copies of the IVUS images were saved on a CD-ROM. The data were quantitatively analyzed by two independent observers with two off-line computer-based software systems (VISIATLAS, Terumo). Tissue characterization of neointimal composition was achieved on IB-IVUS using VISIATLAS™. The excellent correlation of IB-IVUS and histology has been reported previously [7–11]. After tracing vessel area, lumen area, and stent area, grayscale IVUS images and IB-IVUS color-coded maps were displayed side-by-side on a monitor. A neointima was defined as the area between the lumen border and the inner border of the stent struts to avoid stent strut artifacts (Fig. 1A3). The images were analyzed by two observers who were blinded to the clinical and procedural characteristics. We applied the manufacturer's default settings on the basis of previous data [9,10,12] to define a range of IB values for neointimal tissue components. According to the signal level, the IB-IVUS analysis classified the color-coded tissue into

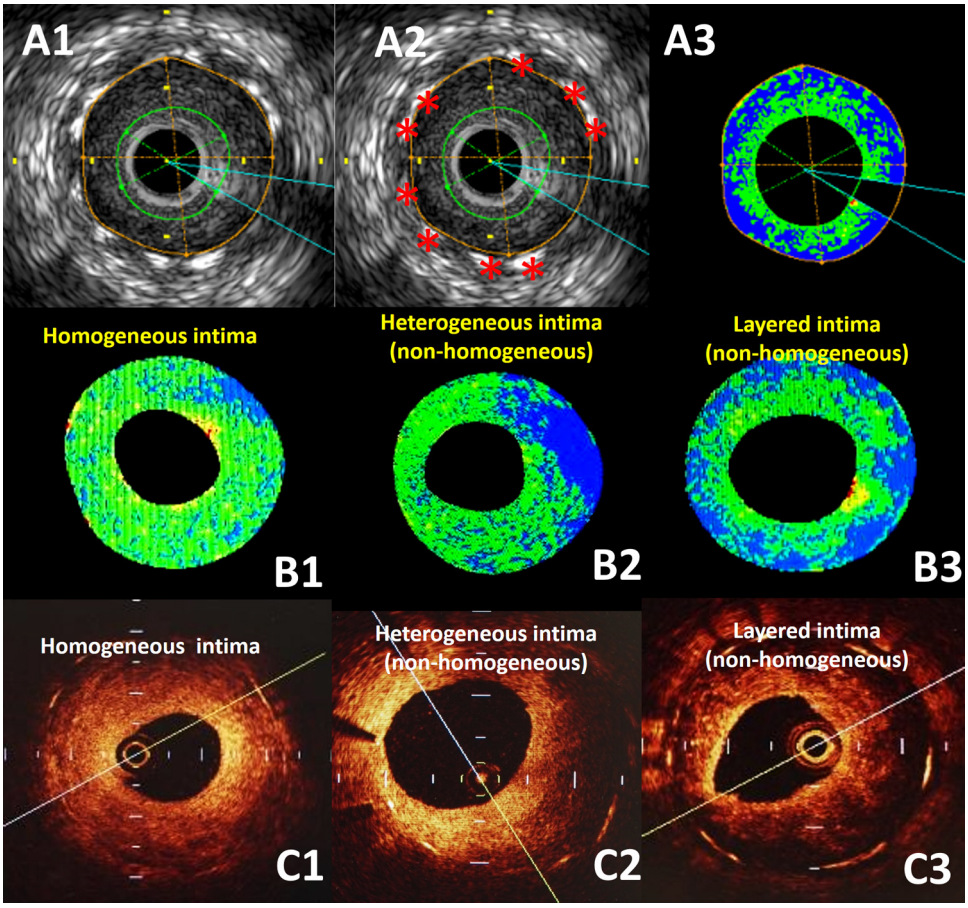

Fig. 1. Gray scale and integrated backscatter intravascular ultrasound (IB-IVUS) and optical coherence tomography (OCT) of in-stent neointima at the area of in-stent restenosis (ISR). (A) Neointima (A3) was defined as the area between the lumen border and the inner border of the stent struts (asterisk) to avoid stent strut artifacts. (B) IB-IVUS analysis: fibrous area (green), lipid area (blue), mixed area (yellow), and calcification (red). The pattern of neointima tissue component was classified into two groups: homogeneous pattern (B1) and non-homogeneous pattern (B2 and B3) according to neointima lipid distribution. (C) Pattern of ISR neointima as assessed by OCT. The pattern of neointima tissue component was classified into two groups: homogeneous pattern (C1) and non-homogeneous pattern (C2 and C3) according to neointima lipid distribution. Both the (B) and (C) images were obtained at the same cross-section. (For interpretation of the references to color in this figure legend, the reader is referred to the web version of this article.)

four major components: red (calcification), yellow (dense fibrosis), green (fibrosis), and blue (lipid). Each component of neointima tissue was represented as a percentage of measured total neointima and the pattern of neointima was classified into two groups according to the difference of lipid distribution in the neointima: (1) homogeneous neointima, characterized by the absence of a lipid pool and a layered structure (Fig. 1B1) and (2) non-homogeneous neointima which is further subdivided into two patterns: (a) heterogeneous neointima characterized by the presence of a lipid pool (Fig. 1B2) and (b) layered neointima with mainly fibrous tissue on the surface and mainly lipid tissue at the bottom but no lipid pool (Fig. 1B3). IB-IVUS-derived thin cap fibroatheroma (IB-IVUS TCFA) was defined as a plaque with percentage lipid pool area ≥55% as previously described [13].

OCT measurements

After performing the IB-IVUS analysis, OCT images were obtained (LightLab Imaging Inc., Westford, MA, USA). A 0.016 in. wire-type imaging catheter (ImagingWire; LightLab Imaging Inc.) was advanced to the distal end of the stent through a 4 Fr over-the-wire occlusion balloon catheter (Helios™; LightLab Imaging). The occlusion balloon was then inflated to 0.3 atm, while lactated Ringer's solution was infused from the balloon tip at 0.5 ml/s to flush the blood from the imaging field. The entire stent was imaged with an automatic pullback device moving at 1.5 mm/s. The OCT measurements were performed at the cross-sections determined by IVUS. The identical cross-sections were carefully selected with the use of intravascular and perivascular landmarks and a constant pullback speed as previously reported [14].

The OCT pattern of neointima was classified into two groups: (1) homogeneous pattern (Fig. 1C1) and (2) non-homogeneous pattern, which further included two distinctive patterns (a) heterogeneous pattern (Fig. 1C2) and (b) layered pattern (Fig. 1C3). This classification has been described in detail elsewhere [14]. To describe the morphologic appearance of the neointima further, restenotic tissue backscatter, lumen shape, intra-luminal material, and the presence of microvessels were also analyzed for each slice in the ISR lesions (Fig. 2). The images were analyzed by two observers who were blinded to the clinical and procedural characteristics. Using the already validated criteria for plaque characterization [2], the minimum fibrous cap thickness was measured at its thinnest part. OCT-derived TCFA was defined as a plaque with a fibrous cap of <65 μm according to previous reports [15]. If the fibrous cap of a given plaque was visible, the thickness of the cap was measured five times and the average of the three middle values was calculated. Calcification was defined as a well-delineated, signal-poor mass with a sharp border [16,17].

IB-IVUS-OCT findings co-registration and analysis

OCT slices of the minimal stent area (MSA) corresponding to the MSA obtained from IB-IVUS were selected for analysis. IB-IVUS and OCT images were acquired at five cross-sections: at the minimal lumen area site and at 1 and 2 mm proximal and distal to the MSA site. Each slice proximal and distal to the MSA site obtained with IB-IVUS and OCT was selected per 1 mm by using the pullback speed and frame numbers. Moreover, in order to obtain corresponding images of IB-IVUS and OCT, the distances from at least two landmarks, such as side branches and/or calcifications, were also used as references. Thus each slice was matched between IB-IVUS and OCT precisely. A total of 120 cross-sections including 40 early restenoses cross-sections (identified at <12 months) and 80 late restenoses cross-sections (identified at ≥12 months) of either BMS ($n = 15$, 75 cross-sections) or DES ($n = 9$, 45 cross-sections) were evaluated in this study.

Statistical analysis

All values are expressed as mean ± SD (continuous variables) or as absolute numbers and percentages (categorical variables). Continuous variables were compared with the unpaired t-test. Categorical variables were compared with chi-square statistics or Fisher's exact test. All p-values are two-sided, and p-values <0.05 were considered statistically significant. The agreement between the pattern of ISR neointima by OCT and that by IB-IVUS was quantified by Cohen's kappa test for concordance. A kappa value of 0.61–0.80 indicates good agreement, and 0.81–1.0 indicates excellent agreement. A kappa test was also used to assess the inter-observer and intra-observer variability for qualitative OCT and IB-IVUS assessments. All statistical analyses were performed using Statview 5.0 (SAS Institute, Cary, NC, USA).

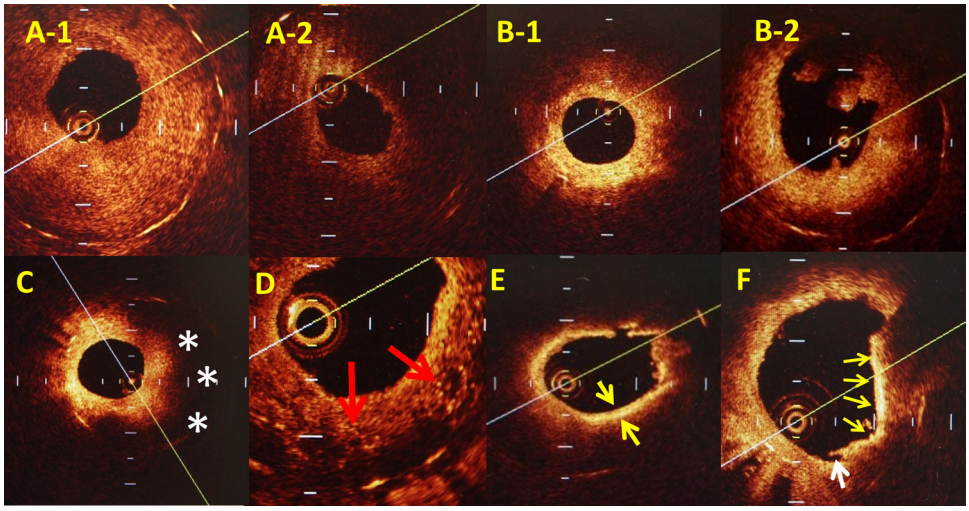

Fig. 2. Qualitative optical coherence tomography (OCT) assessment of in-stent restenosis. To evaluate the morphologic appearance of the restenotic tissue, parameters were defined as follows: high restenotic tissue backscatter (A-1) or low restenotic tissue backscatter (A-2), regular lumen shape (B-1) or irregular lumen shape (B-2), lipid-laden neointima containing (C), visible microvessels (D), thin-cap fibroatheroma (TCFA) (E), intimal rupture/TCFA (F). Asterisks (*) indicate lipid pool. Red arrows indicate microvessels. Yellow arrows indicate TCFA. TCFA was defined as a plaque with a fibrous cap of <65 μm and lipid content in ≥1 quadrant. White arrow indicates intimal rupture surrounded by TCFA-like neointima. (For interpretation of the references to color in this figure legend, the reader is referred to the web version of this article.)

Table 1
Baseline characteristics.

	BMS group ($n=15$)	DES group ($n=9$)	p-Value
Age, years	68.1 ± 9.9	63.8 ± 8.2	0.29
Male, n (%)	14 (93.3)	9 (100)	0.43
Diabetes mellitus, n (%)	6 (40)	5 (56)	0.46
Hyperlipidemia, n (%)	11 (73)	7 (78)	0.80
Hypertension, n (%)	14 (93.3)	8 (88.9)	0.70
Smoking, n (%)	6 (40)	6 (67)	0.20
Left ventricular ejection fraction, %	59.8 ± 12.0	50.8 ± 11.2	0.08
Previous myocardial infarction, n (%)	10 (66.7)	8 (88.9)	0.22
Previous coronary bypass, n (%)	0	2 (22.2%)	0.06
Follow up duration, mo	69.7 ± 56.2	29.4 ± 25.1	<0.01
Laboratory data			
Total cholesterol, mg/dL	167.8 ± 21.2	177.8 ± 39.4	0.43
LDL cholesterol, mg/dL	92.4 ± 20.9	96.0 ± 26.7	0.71
HDL cholesterol, mg/dL	51.5 ± 18.9	42.3 ± 13.1	0.21
TG, mg/dL	117.9 ± 68.1	176.7 ± 85.9	0.08
LDL/HDL cholesterol ratio	2.0 ± 0.8	2.6 ± 1.2	0.21
HemoglobinA1c, %	6.0 ± 0.7	6.3 ± 0.7	0.40
Medications			
Ca antagonist	9 (60.0)	4 (44.4)	0.46
β-Blocker	11 (73.3)	8 (88.9)	0.36
ACE-I/ARB	12 (80.0)	6 (66.7)	0.47
Statin	12 (80)	8 (88.9)	0.57
Stent information			
Stent size, mm	3.5 ± 0.3	2.7 ± 0.3	<0.01
Stent length, mm	21.5 ± 9.4	23.6 ± 4.0	0.54
Types of drug-eluting stent			
Sirolimus		5 (56)	
Paclitaxel		2 (22)	
Everolimus		2 (22)	

Data are presented as no. (%) or mean ± SD.
BMS, bare metal stent; DES, drug-eluting stent; LDL, low-density lipoprotein; HDL, high-density lipoprotein; TG, triglyceride; ACE-I, angiotensin-converting enzyme inhibitor; ARB, angiotensin receptor blockers.

Results

Clinical and procedural characteristics are shown in Table 1. Fifteen patients had restenosis after BMS implantation, and 9 patients after DES implantation (5 patients treated with sirolimus-eluting stents, 2 patients treated with paclitaxel-eluting stents, and 2 patients treated with everolimus-eluting stents). Patient characteristics were not significantly different between the BMS and DES groups. Overall follow-up duration from stent implantation to ISR was 53.6 ± 49.1 months, with the follow-up duration in the group treated with BMS being longer than that in the group treated with DES (69.7 ± 56.2 months, 29.4 ± 25.1 months, $p < 0.01$). The stent size was significantly greater in the BMS group, with stent length being similar between the two groups. A total of 120 cross-sections from the 24 patients who underwent TLR were divided into four groups according to the time at which the restenosis was identified (early phase or late phase) and stent type (BMS or DES). The stent and lumen areas at the each cross-section were significantly different among the four groups, whereas intimal hyperplasia (IH) area was similar in each group according to conventional IVUS analysis

Table 2
Conventional IVUS and IB-IVUS data (early phase < 12 months or late phase ≥12 months).

	BMS group (75 cross-sections)			DES group (45 cross-sections)			p-Value† (early restenosis BMS vs. DES)	p-Value‡ (late restenosis BMS vs. DES)
	Early (15 cross-sections)	Late (60 cross-sections)	p-Value*	Early (25 cross-sections)	Late (20 cross-sections)	p-Value**		
Tissue coverage structure								
Homogeneous, n (%)	10 (66.7)	37 (61.7)	0.52	9 (36)	4 (20)	0.24	0.06	<0.01
Non-homogeneous, n (%)	5 (33.3)	23 (38.3)		16 (64)	16 (80)			
Heterogeneous, n (%)	0	10 (16.7)		6 (24)	8 (40)			
Layered, n (%)	5 (16.7)	13 (21.7)		10 (40)	8 (40)			
Quantitative analysis								
Stent area, mm^2	7.8 ± 0.6	8.2 ± 2.2	0.42	7.3 ± 1.4	9.8 ± 3.3	0.02	0.18	0.02
IH area, mm^2	5.1 ± 0.7	5.2 ± 1.9	0.74	4.6 ± 1.6	5.8 ± 3.3	0.12	0.30	0.33
Lumen area, mm^2	2.7 ± 0.9	3.0 ± 1.3	0.40	2.6 ± 0.8	3.9 ± 1.6	0.01	0.81	0.02
Lesion length, mm	12.5 ± 1.6	12.4 ± 3.9	0.95	7.4 ± 2.8	10.1 ± 3.1	0.23	0.03	0.23
Fibrous neointima, %	65.9 ± 8.1	51.8 ± 12.0	<0.01	65.2 ± 6.5	54.5 ± 12.7	<0.01	0.76	0.39
Lipid neointima, %	28.5 ± 9.7	35.8 ± 14.0	0.06	24.1 ± 10.7	37.0 ± 13.9	<0.01	0.21	0.76
Mixed neointima, %	4.8 ± 3.2	8.9 ± 6.6	0.02	10.1 ± 7.0	7.7 ± 3.8	0.46	<0.01	0.46
Calcification, %	0.8 ± 0.9	3.5 ± 3.3	<0.01	0.5 ± 0.3	0. 9 ± 0.4	<0.01	0.17	<0.01

Data are presented as no. (%) or mean ± SD.
IB-IVUS, integrated backscatter intravascular ultrasound; BMS, bare metal stent; DES, drug-eluting stent; IH area, intimal hyperplasia area.
p-Value*: early phase vs. late phase in BMS. p-Value**: early phase vs. late phase in DES. p-Value†: BMS vs. DES in early phase. p-Value‡: BMS vs. DES in late phase.

(Table 2). The length of the ISR lesion in the early DES restenosis was significantly shorter than that in the BMS early restenosis (7.4 ± 2.8 mm vs. 12.5 ± 1.6 mm, $p = 0.03$).

Tissue component ratios in BMS and DES restenotic neointima as assessed by IB-IVUS

Considering the pattern of neointima as classified by IB-IVUS, DES restenosis was characterized by a non-homogeneous pattern as compared to BMS restenosis, especially in the case of late restenosis (38.3% vs. 80.0%, $p < 0.01$). Percentage fibrous neointima in early BMS restenosis was higher than that in late BMS restenosis (65.9 ± 8.1% vs. 51.8 ± 12.0%, $p < 0.01$) with a trend toward a higher percentage of lipid neointima in late restenosis (28.5 ± 9.7% vs. 35.8 ± 14.0%, $p = 0.06$) (Table 2). Percentage lipid neointima in early DES restenosis on the other hand was significantly lower than that in late DES restenosis (24.1 ± 10.7% vs. 37.0 ± 13.9%, $p < 0.01$). Percentage calcification in late restenosis was significantly greater than that in early restenosis in both the stent types. Moreover, the presence of calcium in BMS late restenosis was greater than that in the DES equivalent (3.5 ± 3.3% vs. 0.9 ± 0.4%, $p < 0.01$). The intra-observer and inter-observer agreement for the ISR IB-IVUS pattern was within an acceptable range (intra-observer; kappa = 0.96, inter-observer; kappa = 0.91, respectively).

Tissue characterization of BMS and DES restenotic neointima as assessed by OCT

As the case with IB-IVUS, OCT identified a more non-homogeneous neointima in DES-ISR as compared to BMS-ISR, especially with regard to late restenosis. More specifically, a non-homogeneous pattern, low backscatter, and lipid-laden neointima was more frequently observed in late DES restenosis as compared to the BMS equivalent (45% vs. 80%, $p < 0.01$; 51.7% vs. 85%, $p < 0.01$; 33.3% vs. 65% $p = 0.01$, respectively). Visible microvessels and lipid-laden neointima were seen more frequently in early DES restenosis as compared to early BMS restenosis (0% vs. 56%, $p < 0.01$, 0% vs. 24%, $p = 0.04$) (Table 3). Visible microvessels and lipid-laden intima neointima were also more commonly observed in late BMS restenosis as compared to early BMS restenosis. Overall, visible microvessels were more frequently observed in the non-homogeneous group by IB-IVUS (28.3% in homogeneous pattern vs. 60.0% in non-homogeneous pattern, $p < 0.01$) (Fig. 3). The intra-observer and inter-observer agreements for the ISR OCT signal pattern was within an acceptable range (intra-observer, kappa = 0.96; inter-observer, kappa = 0.91, respectively).

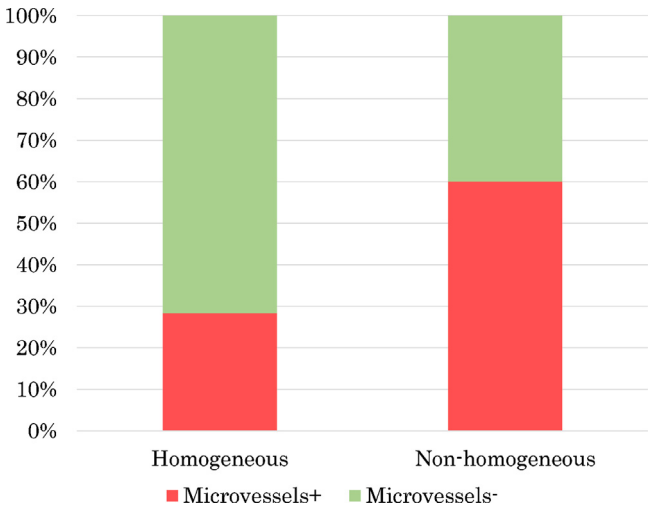

Fig. 3. Comparison of the optical coherence tomography-derived microvessels between the homogeneous and non-homogeneous patterns by integrated backscatter intravascular ultrasound.

Comparison between IB-IVUS and OCT findings

The pattern of ISR neointima (i.e. homogenous vs. non-homogeneous) as identified by IB-IVUS was similar to that identified by OCT. The overall agreement between the pattern of ISR neointima by IB-IVUS and that by OCT was excellent (kappa = 0.85, 95% CI 0.76–0.94) (Table 4). In more detail, both IB-IVUS and OCT identified a predominant non-homogeneous pattern in the ISR neointima of DES restenosis, whereas the ISR neointima of BMS restenosis was characterized by a homogeneous pattern according to both IB-IVUS and OCT. Moreover, regarding the detection of TCFA, the agreement between IB-IVUS-derived TCFA [7.5% (9/120)]

Table 3
OCT qualitative assessment (early phase <12 months or late phase ≥12 months).

	BMS group (75 cross-sections)			DES group (45 cross-sections)			*p*-Value† (Early restenosis BMS vs. DES)	*p*-Value‡ (Late restenosis BMS vs. DES)
	Early (15 cross-sections)	Late (60 cross-sections)	*p*-Value*	Early (25 cross-sections)	Late (20 cross-sections)	*p*-Value**		
Tissue coverage structure								
Homogeneous, *n* (%)	9 (60)	33 (55)	0.72	9 (36)	4 (20)	0.24	0.14	<0.01
Non-homogeneous, *n* (%)	6 (40)	27 (45)		16 (64)	16 (80)			
Heterogeneous, *n* (%)	1 (6.7)	13 (21.7)		13 (52)	5 (25)			
Layered, *n* (%)	5 (33.3)	14 (23.3)		3 (12)	11 (55)			
Backscatter								
High, *n* (%)	7 (46.6)	29 (48.3)	0.55	12 (48)	3 (15)	0.02	0.93	<0.01
Low, *n* (%)	8 (53.3)	31 (51.7)		13 (52)	17 (85)			
Lumen shape								
Regular, *n* (%)	10 (66.7)	51 (85)	0.10	22 (88)	20 (100)	0.10	0.10	0.07
Irregular, *n* (%)	5 (33.3)	9 (15)		3 (12)	0			
Intra-luminal material								
Microvessels, *n* (%)	0	26 (57.8)	<0.01	14 (56)	13 (65)	0.54	<0.01	0.10
Lipid-laden neointima, *n* (%)	0	20 (33.3)	<0.01	6 (24)	13 (65)	<0.01	0.04	0.01
TCFA neointima, *n* (%)	0	10 (16.7)	0.09	1 (4)	4 (20)	0.08	0.32	0.73

Data are presented as no. (%) or mean ± SD.
OCT, optical coherence tomography; BMS, bare metal stent; DES, drug-eluting stent; TCFA, thin-cap fibroatheroma.
p-Value*: early phase vs. late phase in BMS. *p*-Value**: early phase vs. late phase in DES. *p*-Value†: BMS vs. DES in early phase. *p*-Value‡: BMS vs. DES in late phase.

Table 4
Comparison between IB-IVUS classification and OCT classification.

	Early phase (<12months)				Late phase (≥12months)			
	BMS (15 cross-sections)		DES (25 cross-sections)		BMS (60 cross-sections)		DES (20 cross-sections)	
	IB-IVUS	OCT	IB-IVUS	OCT	IB-IVUS	OCT	IB-IVUS	OCT
Homogeneous pattern, *n* (%)	10(66.7)	9 (60)	9(36)	9 (36)	37(61.7)	33 (55)	4(20)	4 (20)
Non-homogeneous pattern, *n* (%)	5(33.3)	6 (40)	16(64)	16 (64)	23(38.3)	27 (45)	16(80)	16 (80)

	OCT classification[a]		
	Homogeneous pattern (55 cross-sections)	Non-homogeneous pattern (65 cross-sections)	Total
IB-IVUS classification			
Homogeneous pattern (60 cross-sections)	53	7	60
Non-homogeneous pattern (60 cross-sections)	2	58	60
Total	55	65	120

Data are presented as no. (%).
IB-IVUS, integrated backscatter intravascular ultrasound; OCT, optical coherence tomography; BMS, bare metal stent; DES, drug-eluting stent.
[a] Cohen's kappa = 0.85 (95% CI 0.75–0.94).

Table 5
Comparison between IB-IVUS-derived TCFA and OCT-derived TCFA.

	OCT-derived TCFA+ (15 cross-sections)[a]	OCT-derived TCFA− (105 cross-sections)[a]	Total
IB-IVUS-derived TCFA+ (9 cross-sections)	8	1	9
IB-IVUS-derived TCFA− (111 cross-sections)	7	104	111
Total	15	105	120

IB-IVUS, integrated backscatter intravascular ultrasound; TCFA, thin cap fibroatheroma; OCT, optical coherence tomography.
[a] Cohen's kappa = 0.63 (95% CI 0.39–0.88).

and OCT-derived TCFA [12.5% (15/120)] was good (kappa = 0.63, 95%CI 0.39–0.88) (Table 5).

Procedure outcomes

The slow flow (SF) phenomenon occurred in five lesions [BMS vs. DES: 11.1% (1/15) vs. 44.4% (4/9)]. Moreover, this phenomenon occurred more frequently at MSA sites with a non-homogeneous pattern [homogeneous pattern by IB-IVUS vs. non-homogeneous pattern by IB-IVUS: 0% (0/9) vs. 33.3% (5/15), $p = 0.02$]. Percentage lipid neointima by IB-IVUS was greater in the non-homogeneous than in the homogeneous pattern ($38.0 \pm 13.0\%$ vs. $27.3 \pm 12.3\%$, $p < 0.01$). Recurrent ISR occurred in six lesions [BMS vs. DES: 22.2% (2/15) vs. 44.4% (4/9)] with all of these lesions demonstrating anon-homogeneous pattern at the MSA site [homogeneous pattern by IB-IVUS vs. non-homogeneous pattern by IB-IVUS: 0% (0/9) vs. 40.0% (6/15), $p < 0.01$].

Discussion

This study aimed to qualitatively evaluate ISR neointima by IB-IVUS and examine how this evaluation compares to OCT. Our major findings are:

(1) The evaluation of neointima morphology by IB-IVUS revealed similar findings as that by OCT.
(2) The neointima of late DES restenosis, in contrast to that of late BMS restenosis is characterized by a non-homogeneous pattern according to both IB-IVUS and OCT.

Previous OCT studies have suggested that neoatherosclerosis including the presence of a lipid-laden neointima is more frequently detected in DES late restenosis as compared to the BMS equivalent [6,18,19]. Furthermore, histological studies have suggested that in a significant proportion of DES, neoatherosclerotic changes can be seen as early as 9 months after implantation, whereas in BMS this process tends to be less aggressive and to occur much later [20]. The atherosclerotic progression may be related to dysfunctional endothelium leading to neointimal rupture and very late stent thrombosis (VLST), which occurs more frequently in DES as compared to BMS [20,21]. Similar results were observed in our study where a predominant non-homogeneous neointima was identified in late DES restenosis. This is suggestive of a predominant neoatherosclerotic process in late DES restenosis. In contrast, late BMS restenosis was characterized by a pattern suggestive of both neointimal hyperplasia and neoatherosclerosis. The relatively high prevalence of non-homogeneous tissue restenosis that we found in DES and the very low occurrence of VLST suggest that other unknown factors come into play.

Comparison with previous studies utilizing IB-IVUS

Muraoka et al. [22] have reported a subgroup of DES restenosis with low backscatter value (allegedly-corresponding to lipid) in which distal SF was observed after balloon angioplasty (POBA). In our study, SF occurred more frequently at MSA sites with a non-homogeneous pattern where the percentage lipid neointima was found to be greater as compared to sites with a homogeneous pattern. Thus, the results of our study are in agreement with the findings of the aforementioned study.

Comparison with previous study utilizing virtual histology-IVUS

In our study, the percentage lipid neointima in late phase restenosis was higher than that in early phase restenosis (BMS: $35.8 \pm 14.0\%$ vs. $28.5 \pm 9.7\%$, $p = 0.06$; DES: $37.0 \pm 13.9\%$ vs. $24.1 \pm 10.7\%$, $p < 0.01$). Percentage calcification in late restenosis was also significantly greater than that in early restenosis, again in both stent types (BMS: $3.5 \pm 3.3\%$ vs. $0.8 \pm 0.9\%$, $p < 0.01$; DES: $0.9 \pm 0.4\%$ vs. $0.5 \pm 0.3\%$, $p < 0.01$). Although the absence of a clear definition for necrotic core by IB-IVUS makes it extremely difficult to compare these observations to those obtained by virtual

histology (VH)-IVUS, our results seem to be in agreement with the VH-IVUS study of Kang et al. [23], who demonstrated that BMS- and DES-treated lesions can subsequently develop an in-stent necrotic core and dense calcium, both of which are suggestive of neoatherosclerosis.

Comparison with previous study utilizing iMAP

Tsujita et al. [24] reported that DES implantation can be associated with more iMAP-derived necrotic and less-fibrotic neointimal formation compared with BMS implantation. In our study, however, there was no significant difference between percentage lipid and fibrous neointima in DES restenosis as compared to BMS restenosis. These findings are consistent with the results of IB-IVUS analysis by Muraoka et al. [22]. The discrepancy between the two modalities could be related to differences in definitions for tissue characterization.

In our study, although OCT provided a detailed evaluation of the neointima in ISR lesions, IB-IVUS gave a similar accurate assessment of neointima morphology. The two modalities agreed regarding the pattern of restenosis in BMS and DES irrespective of the timing. These findings suggest that IB-IVUS can be used to evaluate neointimal morphology especially in situations where contrast volume needs to be kept at a minimum or when the assessment of vessel size is important. It may also be a useful tool for stratifying the risk of developing SF after plain-old balloon angioplasty as well as recurrent ISR by detecting a non-homogeneous pattern. Our results will need to be validated by a specific histological study.

Conclusion

This study indicates that the use of IB-IVUS in patients with stable angina can provide similar information regarding the pattern of ISR neointima as the gold-standard OCT. Both modalities suggested that late DES restenosis is characterized by a non-homogeneous lipid neointima as compared to that observed in the BMS equivalent, which could be one of the reasons behind the VLST observed with DES. Larger studies are required to validate these findings.

Limitations

This study was a single-center investigation based on a relatively small sample size. The use of native atherosclerosis criteria for the characterization of ISR neointima may lead to significant misclassification as the color-coded classification of IB-IVUS is based on the histology of native coronary plaques. Moreover, we excluded acute coronary syndrome patients in whom ISR neointima is more likely to include TCFA and thrombus [25]. We cannot therefore conclude that IB-IVUS can provide similar detailed information regarding the ISR neointima pattern in these patients. A validation study comparing the histology of ISR neointima and IB-IVUS findings is needed in the future. We could not directly compare the differences at the same time interval after implantation between the neointima of late BMS and late DES restenosis because of the differences in the time-periods that these were identified. Finally, we cannot comment on the natural history of neointima progression as serial studies of the same implanted stent were not performed and we cannot conclusively state that neointima composition plays a role in determining clinical events.

Source of funding

None.

Conflict of interest

None.

References

[1] Kawasaki M, Takatsu H, Noda T, Sano K, Ito Y, Hayakawa K, Tsuchiya K, Arai M, Nishigaki K, Takemura G, Minatoguchi S, Fujiwara T, Fujiwara H. In vivo quantitative tissue characterization of human coronary arterial plaques by use of integrated backscatter intravascular ultrasound and comparison with angioscopic findings. Circulation 2002;105:2487–92.
[2] Yabushita H, Bouma BE, Houser SL, Aretz HT, Jang IK, Schlendorf KH, Kauffman CR, Shishkov M, Kang DH, Halpern EF, Tearney GJ. Characterization of human atherosclerosis by optical coherence tomography. Circulation 2002;106:1640–5.
[3] Kubo T, Nakamura N, Matsuo Y, Okumoto Y, Wu X, Choi SY, Komukai K, Tanimoto T, Ino Y, Kitabata H, Kimura K, Mizukoshi M, Imanishi T, Akagi H, Yamamoto T, et al. Virtual histology intravascular ultrasound compared with optical coherence tomography for identification of thin-cap fibroatheroma. Int Heart J 2011;52:175–9.
[4] Okubo M, Kawasaki M, Ishihara Y, Takeyama U, Yasuda S, Kubota T, Tanaka S, Yamaki T, Ojio S, Nishigaki K, Takemura G, Saio M, Takami T, Fujiwara H, Minatoguchi S. Tissue characterization of coronary plaques: comparison of integrated backscatter intravascular ultrasound with virtual histology intravascular ultrasound. Circ J 2008;72:1631–9.
[5] Goto K, Takebayashi H, Kihara Y, Hagikura A, Fujiwara Y, Kikuta Y, Sato K, Kodama S, Taniguchi M, Hiramatsu S, Haruta S. Appearance of neointima according to stent type and restenotic phase: analysis by optical coherence tomography. EuroIntervention 2013;9:601–7.
[6] Nagoshi R, Shinke T, Otake H, Shite J, Matsumoto D, Kawamori H, Nakagawa M, Kozuki A, Hariki H, Inoue T, Ohsue T, Taniguchi Y, Iwasaki M, Nishio R, Hiranuma N, et al. Qualitative and quantitative assessment of stent restenosis by optical coherence tomography: comparison between drug-eluting and bare-metal stents. Circ J 2013;77:652–60.
[7] Ohota M, Kawasaki M, Ismail TF, Hattori K, Serruys PW, Ozaki Y. A histological and clinical comparison of new and conventional integrated backscatter intravascular ultrasound (IB-IVUS). Circ J 2012;76:1678–86.
[8] Kawasaki M. In vivo quantitative tissue characterization of human coronary arterial plaques by use of integrated backscatter intravascular ultrasound and comparison with angioscopic findings. Circulation 2002;105:2487–92.
[9] Okubo M, Kawasaki M, Ishihara Y, Takeyama U, Kubota T, Yamaki T, Ojio S, Nishigaki K, Takemura G, Saio M, Takami T, Minatoguchi S, Fujiwara H. Development of integrated backscatter intravascular ultrasound for tissue characterization of coronary plaques. Ultrasound Med Biol 2008;34:655–63.
[10] Ando H, Amano T, Takashima H, Harada K, Kitagawa K, Suzuki A, Kunimura A, Shimbo Y, Harada K, Yoshida T, Kato B, Uetani T, Kato M, Matsubara T, Kumagai S, et al. Differences in tissue characterization of restenotic neointima between sirolimus-eluting stent and bare-metal stent: integrated backscatter intravascular ultrasound analysis for in-stent restenosis. Eur Heart J Cardiovasc Imaging 2013;14:996–1001.
[11] Nakayama N, Hibi K, Endo M, Miyazawa A, Suzuki H, Maejima N, Isshiki T, Kozuma K, Kimura K. Validity and reliability of new intravascular ultrasound analysis software for morphological measurement of coronary artery disease. Circ J 2013;77:424–31.
[12] Kawasaki M, Hattori A, Ishihara Y, Okubo M, Nishigaki K, Takemura G, Saio M, Takami T, Minatoguchi S. Tissue characterization of coronary plaques and assessment of thickness of fibrous cap using integrated backscatter intravascular ultrasound. Circ J 2010;74:2641–8.
[13] Miyamoto Y, Okura H, Kume T, Kawamoto T, Neishi Y, Hayashida A, Yamada R, Imai K, Saito K, Yoshida K. Plaque characteristics of thin-cap fibroatheroma evaluated by OCT and IVUS. JACC Cardiovasc Imaging 2011;4:638–46.
[14] Yamada R, Okura H, Kume T, Saito K, Miyamoto Y, Imai K, Tsuchiya T, Maehama T, Okahashi N, Obase K, Hayashida A, Neishi Y, Kawamoto T, Yoshida K. Relationship between arterial and fibrous cap remodeling: a serial three-vessel intravascular ultrasound and optical coherence tomography study. Circ Cardiovasc Interv 2010;3:484–90.
[15] Gonzalo N, Serruys PW, Okamura T, van Beusekom HM, Garcia-Garcia HM, van Soest G, van der Giessen W, Regar E. Optical coherence tomography patterns of stent restenosis. Am Heart J 2009;158:284–93.
[16] Jang IK, Tearney GJ, MacNeill B, Takano M, Moselewski F, Iftima N, Shishkov M, Houser S, Aretz HT, Halpern EF, Bouma BE. In vivo characterization of coronary atherosclerotic plaque by use of optical coherence tomography. Circulation 2005;111:1551–5.
[17] Yabushita H. Characterization of human atherosclerosis by optical coherence tomography. Circulation 2002;106:1640–5.
[18] Kim JS, Hong MK, Shin DH, Kim BK, Ko YG, Choi D, Jang Y. Quantitative and qualitative changes in des-related neointimal tissue based on serial oct. JACC Cardiovasc Imaging 2012;5:1147–55.
[19] Habara M, Terashima M, Nasu K, Kaneda H, Yokota D, Ito T, Kurita T, Teramoto T, Kimura M, Kinoshita Y, Tsuchikane E, Asakura Y, Suzuki T. Morphological differences of tissue characteristics between early, late, and very late restenosis lesions after first generation drug-eluting stent implantation: an optical coherence tomography study. Eur Heart J Cardiovasc Imaging 2013;14:276–84.

[20] Nakazawa G, Otsuka F, Nakano M, Vorpahl M, Yazdani SK, Ladich E, Kolodgie FD, Finn AV, Virmani R. The pathology of neoatherosclerosis in human coronary implants bare-metal and drug-eluting stents. J Am Coll Cardiol 2011;57:1314–22.
[21] Kubo S, Kadota K, Ozaki M, Ichinohe T, Eguchi H, Miyake K, Hyodo Y, Saito N, Otsuji H, Otsuru S, Hasegawa D, Shigemoto Y, Habara S, Tada T, Tanaka H, et al. Difference in clinical and angiographic characteristics of very late stent thrombosis between drug-eluting and bare-metal stent implantations. Circ J 2013;77:1453–60.
[22] Muraoka Y, Sonoda S, Kashiyama K, Kamezaki F, Tsuda Y, Araki M, Okazaki M, Otsuji Y. Evaluation of in-stent neointimal tissue components using integrated backscatter intravascular ultrasound: comparison of drug-eluting stents and bare-metal stents. Int J Cardiovasc Imaging 2012;28:1635–41.
[23] Kang SJ, Mintz GS, Park DW, Lee SW, Kim YH, Lee CW, Han KH, Kim JJ, Park SW, Park SJ. Tissue characterization of in-stent neointima using intravascular ultrasound radiofrequency data analysis. Am J Cardiol 2010;106:1561–5.
[24] Tsujita K, Takaoka N, Kaikita K, Hokimoto S, Horio E, Sato K, Mizobe M, Nakayama N, Kojima S, Tayama S, Sugiyama S, Nakamura S, Ogawa H. Neointimal tissue component assessed by tissue characterization with 40 mhz intravascular ultrasound imaging: comparison of drug-eluting stents and bare-metal stents. Catheter Cardiovasc Interv 2013;82:1068–74.
[25] Kang SJ, Mintz GS, Akasaka T, Park DW, Lee JY, Kim WJ, Lee SW, Kim YH, Whan Lee C, Park SW, Park SJ. Optical coherence tomographic analysis of in-stent neoatherosclerosis after drug-eluting stent implantation. Circulation 2011;123:2954–63.